Centrifugal Compressor Stability Prediction Using a New Physics Based Approach

J. Jeffrey Moore

David L. Ransom

Southwest Research Institute,
San Antonio, TX 78238

The accurate prediction of centrifugal compressor stability continues to be an important area of interest in the oil and gas industries. Ensuring stability is critical to the cost-effective installation and operation of these machines in remote environments, where field stability problems are much more expensive to diagnose and correct. Current industry standards and tools for the prediction of impeller destabilizing forces are based on empirical methods that, to date, have served fairly well for systems with reasonable stability margins. However, as stability margins are decreased, use of a modeling method that is more physics based and can better represent the observed trends in machine behavior at low stability margins is required. Furthermore, the development of megaclass liquefied natural gas (LNG) compressors and ultra-high pressure re-injection compressors provides further motivation to improve accuracy. In this paper, a new physics based expression for the prediction of impeller cross-coupling, previously described by Moore et al. ("Rotordynamic Force Prediction of Centrifugal Compressor Impellers Using Computational Fluid Dynamics," ASME Paper No. GT2007-28181), is further investigated by analyzing several classes and scale factors of impellers ranging from 2D designs used in re-injection to full 3D impellers typically used in LNG. The new expression is based on both computational fluid dynamics simulation and experimental test data from a known instability. These results are then applied to two case studies of marginally stable and unstable compressors in the field that were studied by the authors' company. For each case study, the system stability is evaluated using both the new physics based expression as well as the more traditional empirical approaches. Comparisons are made for overall stability prediction as well as sensitivity to system changes. Conclusions are made regarding the applicability and limits of this new approach. [DOI: 10.1115/1.4000113]

1 Introduction

Centrifugal compressors are used in a variety of processes within the natural gas industry. Centrifugal impellers impart work to the gas to increase pressure. As the pressure in the compressor increases, the dynamic behavior at shaft and impeller seals, axial thrust balance pistons, and impellers becomes more significant. Bulk-flow methods have had some success in predicting these aerodynamic forces of centrifugal impellers, but most analysts have relied on the semi-empirical formulations. Many new compressor designs have experienced unexpected and damaging instabilities, resulting in significant lost production and down-time. The current investigation works to develop an improved method of predicted aerodynamic destabilizing cross-coupling forces from centrifugal compressor impellers.

Two types of vibration in industrial compressors are synchronous and subsynchronous vibrations. Synchronous (frequency at running speed) vibrations are normally excited by residual unbalance. The second, more serious type of vibration occurs when nonconservative tangential forces (cross-coupling) act to excite a lateral natural frequency that lies below the running speed, thus the name subsynchronous vibration. These excitation forces generated at seals and impellers have components that act at right angles to the displacement vector. Cross-coupling forces sustain whirling motion at a subsynchronous natural frequency when insufficient damping is present. The whirling motion is referred to as a self-excited rotordynamic instability and can lead to serious internal damage when experienced.

Many well-known instabilities have occurred in the oil and gas industry over the last several decades. A more recent instability of a large LNG propane compressor is described by Memmott [1]. There are also compressors being designed for ultrahigh pressure applications in Kazakhstan and Oman. Given the high cost of oil and natural gas, the potential impact of rotordynamic instability can run in the hundreds of millions of dollars. Therefore, even greater motivation to quantify all destabilizing forces exists today in order to mitigate risk on these large scale projects.

Advancements in computational fluid dynamics (CFD) have permitted detailed fluid dynamic prediction of complex turbulent flows inside turbomachinery. CFD was employed in this study to predict the impeller-fluid reaction forces, which generates the aerodynamic cross-coupling. The procedure utilized in this method was developed for pump impellers by Moore and Palazzolo [2] and showed good correlation to test data. Unfortunately, no direct measurement of rotordynamic coefficients exists for centrifugal compressors. Therefore, in order to validate the present model, comparisons were made to predict the instability of a full scale, industrial centrifugal compressor. Test data for this compressor was obtained from the manufacturer. While this approach is less than ideal, this case study validated the CFD predictions for aerodynamic cross-coupling using real test data. Before the compressor impeller was modeled, the analysis on the pump geometry, identical to that used by Moore and Palazzolo [3], was repeated but using more advanced meshing schemes to verify the model's accuracy.

2 Limitations in the Prediction of Subsynchronous Vibrations

Methods are well established for conducting lateral rotordynamic analyses, which take many potential sources of destabiliz-

Contributed by the International Gas Turbine Institute of ASME for publication in the JOURNAL OF ENGINEERING FOR GAS TURBINES AND POWER. Manuscript received March 19, 2009; final manuscript received August 13, 2009; published online May 20, 2010. Editor: Dilip R. Ballal.

ing and stabilizing forces into account to determine the stability of the composite system. Typically, this is accomplished by developing rotordynamic coefficients for the bearings, seals (especially the balance piston or division wall seal), and impellers. These coefficients essentially function as spring and damper connections between the rotordynamic model of the shaft and the supporting casing. Well-developed computer modeling techniques exist for calculating these stiffness and damping coefficients for bearings and seals. However, for impellers the current state-of-the-art is to estimate the coefficients using approximate empirically based methods.

Wachel and von Nimitz [4] developed an empirical method known as the "Wachel method" using known instability test cases. The empirical Wachel method does not take into account the detailed geometry of the impeller and secondary passages or the first-principle mathematics of compression physics. Nonetheless, on a number of occasions, this method has predicted the presence of subsynchronous vibrations that would not be predicted if the impeller effects were ignored. The Wachel method is widely referenced and has become the current standard for predicting impeller cross-coupling. The American Petroleum Institute's (API) most recent specification [5] for centrifugal compressors requires the use of a variation in the Wachel method to confirm impeller rotordynamic stability. Memmott [1] has created a variation in the Wachel expression, which is used in the current version of API 617 [5]. The need to include impeller cross-coupling in addition to labyrinth seal effects is debated in the industry and will be addressed in this paper.

3 Previous Work to Predict Cross-Coupling Stiffness Values

Moore and Palazzolo [2] demonstrated a CFD based method to determine cross-coupled stiffness for liquid pump impellers. They used a grid perturbation method (GPM) approach in which a 3D structured computational mesh fills the annular space between rotating and stationary members. The rotating impeller was then perturbed radially, and a whirling motion was applied. The mesh conformed to the eccentric surface in a whirling coordinate frame, which rotated with the whirling motion of the rotor. The solution was repeated for multiple whirling frequencies.

Baun [6], at the University of Virginia, employed a commercially available CFD code to predict synchronous axial and radial fluid dynamic forces on a single-stage centrifugal pump. He also compared predicted forces to measurements from magnetic bearing "load cells" on the shaft. However, only cross-coupled stiffness comparisons are presented in this paper.

Other researchers have utilized bulk-flow methods. Childs [7] expanded his incompressible, turbulent, concentric bulk-flow seal model to a variable radius model by solving the axial momentum in the pathwise, meridional direction. The resulting radial impedance curves generated by the bulk-flow analysis showed reasonable results but also exhibited substantial "resonances" for inlet swirls exceeding 0.5. The resonant peaks were attributed to the centrifugal acceleration term in the path momentum equations. Gupta and Childs [8] expanded Childs' model for compressible flow including moment coefficients. Their results were less destabilizing than the Wachel number for the single-stage compressor example studied. Furthermore, Gupta found that the moment coefficient effects were small compared with the radial coefficients. Fulton [9] advocates that labyrinth seals provide the majority of the cross-coupled effects in a turbocompressor and accounting for the effect of impeller shroud forces is not necessary when performing a stability analysis. This paper attempts to address this important issue. More recently, Gupta et al. [10] compared rotor stability predictions to measurements made with a magnetic bearing exciter under factory full-load tests using both bulk-flow and API–Wachel methods. Unfortunately, the rotor analyzed contained a hole-pattern damper seal, which dominates the stability, compared with the impeller cross-coupling effects, making a comparison between the two methods difficult. Moore and Palazzolo [2] compared their CFD results for a pump impeller to the bulk-flow predictions of Childs. The two results are similar for a shroud inlet swirl ratio of 0.5 (CFD predicted 0.52), but the bulk-flow method showed "resonance" behavior over the range of whirling frequencies for a swirl ratio of 0.6, which have not been observed in the CFD results or experiment.

For compressible flows, the energy equation and an equation of state are required to completely describe the fluid flow. The industrial centrifugal impellers considered here are subsonic designs, so the prediction of shocks and their interactions with boundary layers is not required. Moore [11] applied a similar grid perturbation method to gas labyrinth seals with good success.

4 Background

Over the course of the past two years, the authors have worked together with other researchers to develop a more reliable method for estimating the cross-coupled influence of compressor impellers. This work has been published (Moore et al. [12] and Moore and Ransom [13]) and is summarized in this section for the convenience of the reader. The concept of the method is to use CFD to characterize the destabilizing influence of a particular impeller, providing the rotordynamic design engineer a more reliable stability prediction for similar impeller designs. In order to extend the CFD results to other performance conditions or similar impellers of different diameters, a dimensionless cross-coupled coefficient and associated cross-coupled stiffness formula are provided. In this way, the approach of the design engineer remains essentially unchanged, yet enhanced by the use of a physics based approach.

During the development of this new approach, the authors studied the influence of various parameters on the normalization of the CFD calculated cross-coupled stiffness. The authors found that the most important parameters were the discharge density, percent of design flow, tip speed, and geometric length of the impeller shroud. The discharge density accounted for variations in the discharge pressure as well as for variations in the mole weight. Although it seemed reasonable that flow coefficient would be a good normalizing parameter, the authors found that normalizing the flow to the design flow is a more effective parameter. It was further found that tip speed was an important parameter, allowing the results to be applied to cases of varying operating speed. Finally, the authors determined that the projected length of the impeller shroud was a relevant and important normalizing parameter given that the shroud passage contributes the majority of the rotordynamic force.

Based on the parametric study, the authors presented the following formula (referred to as SwRI–CFD) as an alternative formulation to the Wachel equation as follows:

$$k_{xy} = \frac{C_{mr}\rho_d U^2 L_{\text{shr}}}{Q/Q_{\text{design}}} \tag{1}$$

Note that C_{mr} is dimensionless with SI units. This coefficient is nearly constant for a given impeller geometry, but can vary somewhat depending on the detail geometry of the impeller and shroud passage as will be demonstrated later. Equation (1) states that the cross-coupling is proportional to the dynamic pressure ($\rho_d U^2$) and the shroud length (L_{shr}). The cross-coupling is inversely proportional to relative flow. This last factor is due to the increase in swirl exiting the impeller as the relative flow is decreased. Increased swirl in the shroud passage increases the cross-coupled stiffness.

For comparison, the API modified Wachel method [5] (referred to as API–Wachel) is calculated per Eq. (2) as follows:

$$K_{xy} = \left(\frac{189{,}000}{N}\right) \sum \left(\frac{Hp}{D \cdot B_3}\right)\left(\frac{\rho_d}{\rho_s}\right)(\eta^2) \tag{2}$$

Note that Eq. (2) is for use with U.S. customary units. The total cross-coupling is the weighted sum from each impeller based on the modal amplitude of the first forward whirling mode.

The SwRI modified Wachel method (referred to as SwRI–Wachel) is slightly different from the API–Wachel method in two places. First, the SwRI modification includes the fluid mole weight (MW) identical to the original Wachel formulation, whereas the API–Wachel method eliminates the mole weight by setting mole weight equal to 30. Second, the SwRI–Wachel method considers the overall section density ratio (like the Wachel method) not the ratio for each individual stage. Unlike the Wachel method, the SwRI–Wachel method uses individual stage power and dimensions rather than using total or average values. The SwRI–Wachel method is provided in Eq. (3) as follows:

$$K_{xy} = \left(\frac{6300 \cdot MW}{N}\right)\left(\frac{\rho_d}{\rho_s}\right)\sum\left(\frac{Hp}{D \cdot B_3}\right)(\eta^2) \tag{3}$$

where ρ_d and ρ_s represent the discharge and suction densities across the whole compressor section (or whole casing for single section compressor), respectively.

For a straight-through compressor with no side-streams, the SwRI–Wachel method uses the density ratio across the whole machine. Note that all of the cross-coupling values of the Wachel based methods are modally weighted. The same weighting is used for the CFD results using Eq. (4) as follows:

$$K_{xy} = \sum (k_{xy}\eta^2) \tag{4}$$

where k_{xy} is the calculated stage cross-coupling of each impeller calculated using the SwRI–CFD method.

5 Validation Case Study

The initial work was based on a four-stage compressor that was purposely pushed into instability in a factory test environment. The data provided by the manufacturer allowed for complete rotordynamic analysis of the entire system, as well as a full CFD analysis of the impeller design. The details of the CFD analysis are provided by Moore et al. [12]. The test data from the manufacturer included two distinct operating conditions where instability was recorded. These were referred to as Points no. 1 and 2. Using this information, the authors built a CFD model of the compressor impeller and modeled several operating conditions. A rotordynamic model was also built and used to study the stability as a function of impeller excitation. The knowledge gained from this combined work was then used to develop the cross-coupled stiffness formulation presented by Moore et al. [12].

6 Description of CFD Model

Figure 1 shows a 2D view of the compressor mesh with the boundary condition surfaces labeled. No solid model was available from the manufacturer so the solid model was constructed by reverse engineering an actual impeller.

A geometric perturbation of the outer impeller shroud surface was performed, resulting in a sinusoidal clearance function around the circumference. The choice of eccentricity in the CFD simulation was arbitrary but was typically kept near 10% of the shroud clearance to capture the linear, small motion characteristics. This value was determined based on previous modeling of annular seals [14].

Since only shroud forces are of interest in this study, just the shroud region was made eccentric (see Fig. 2). The shroud of the solid model was moved radially while the labyrinth seal remained concentric. The effect of the labyrinth seal was modeled in the rotordynamics model using a traditional bulk-flow seal code.

An unstructured CFD mesh was generated that included both the primary and secondary passages, as shown in Fig. 1. A total pressure condition is specified at the inlet and the velocity components (in cylindrical coordinates) are specified at the exit. This approach assures a uniform velocity field without constraining the discharge pressure and therefore the cross-coupling developed. A solution was obtained using a multiple frame of reference solution where the inlet, diffuser, and shroud passage were solved in the whirling frame of reference, and the primary passage was solved in the rotating frame of reference using ANSYS CFX-5 [15]. Two sliding interfaces using "frozen rotor" assumptions were used, as shown in Fig. 1. Integration of the computed pressures acting on

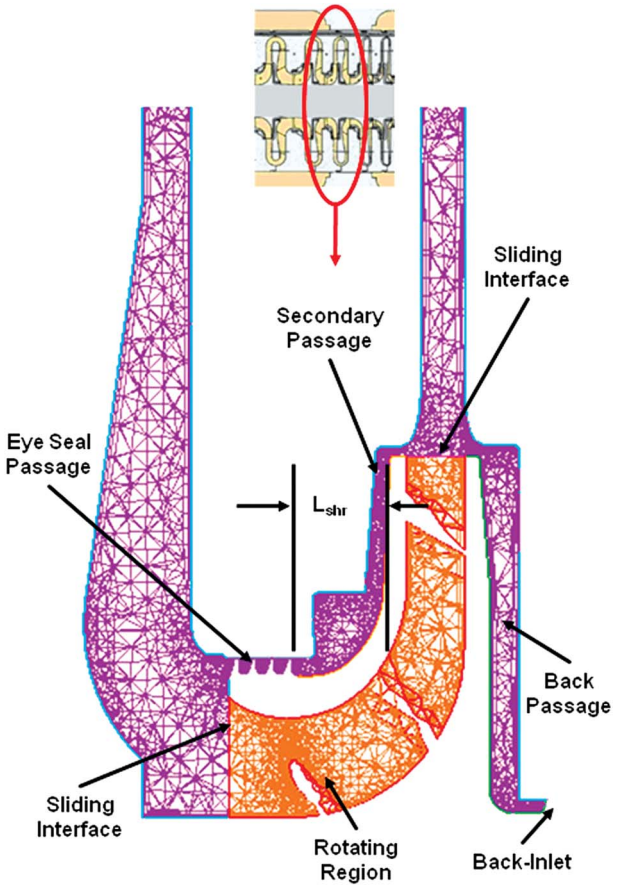

Fig. 1 Compressor impeller mesh showing sliding interfaces

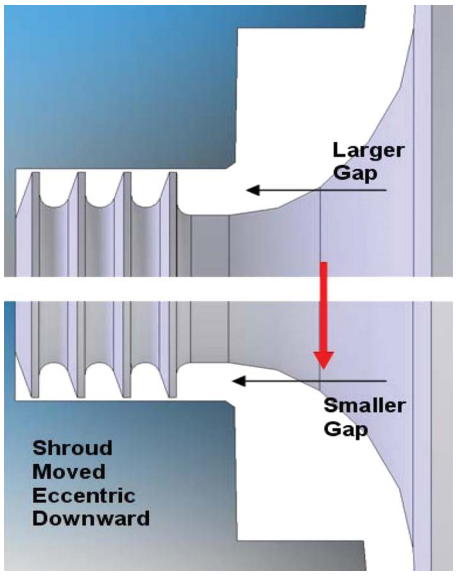

Fig. 2 Eccentric shroud geometry for impeller

Table 1 Summary of derived force coefficients for impeller at instability point no. 1 (21,500 rpm)

		Stage 1		Stage 3	
	Units	Shroud	Eye labyrinth seal	Shroud	Eye labyrinth seal
K_{xx}	(lbf/in.)	−1326	4150	−1623	5980
K_{xy}	(lbf/in.)	2086	3310	3474	5370
C_{xx}	(lbf s/in.)	1.77	1.79	3.25	2.59
C_{xy}	(lbf s/in.)	1.26	−0.65	1.26	−1.03
M_{xx}	(lb)	0.0947	-	0.0790	-
M_{xy}	(lb)	−0.136	-	−0.268	-
WFR_s		0.52	0.82	0.47	0.92

the impeller surfaces resulted in forces both aligned with and transverse to (radial and tangential) the perturbation vector. Dividing these forces with the perturbation eccentricity resulted in rotordynamic impedances that can be curve fit to a second order curve polynomial. The coefficients of this polynomial are the rotordynamic stiffness, damping, and inertia coefficients. A full description of this method can be found in Ref. [12].

The exact conditions for the first instability were obtained from test records. Overall, the CFD results were in reasonable agreement with the performance data, thus validating the model. Since a CFD analysis was performed on only stages 1 and 3, normalized parameters were used to calculate the coefficients for stages 2 and 4. These derived force coefficients were close to the actual CFD values for stages 1 and 3, thus validating the method used. The resulting force coefficients at instability point no. 1 are shown in Table 1. The coefficients are skew symmetric (i.e., $K_{xx}=K_{yy}$, $K_{xy}=-K_{yx}$, etc.). The coefficients calculated separately for the impeller eye labyrinth seals using the bulk-flow code XLLaby are also shown. The magnitude of the shroud forces are of similar magnitude as the impeller eye seal values. These results emphasize the need to include both effects. Table 2 provides the calculated impeller eye labyrinth seal swirl ratios for each stage for both instability points. Note the relatively high swirl ratio for this stage. The whirl frequency ratio of the shroud is near 0.5 for both stages.

Table 2 Summary of predicted impeller eye labyrinth seal inlet swirl ratios using CFD

	Instability point	
Seal	Pt. 1	Pt. 2
Eye 1	0.73	0.69
Eye 2	0.76	0.72
Eye 3	0.78	0.74
Eye 4	0.81	0.77

7 Rotordynamic Modeling of Compressor

A rotordynamic analysis was performed to calculate the stability of the compressor rotor, including the effects of rotor flexibility, bearing stiffness and damping, eye seal stiffness and damping, balance piston stiffness and damping, and aerodynamic excitation using XLTRC^2 [16]. Figure 3 shows the rotor configuration and detail of the rotordynamic model that were found by Moore et al. [12]. The stability analysis was performed by first calculating the potential impeller excitation (cross-coupled stiffness) using three methods. First, the Wachel method discussed above was applied in two different forms. One was the API–Wachel formula and the other was a SwRI–Wachel modification of the same method. The third impeller excitation calculation comes directly from the present CFD work.

As described above, two compressor instability cases were analyzed: instability point no. 1 (21,500 rpm) and instability point no. 2 (23,000 rpm). Even though the speed was increased for point 2, the discharge pressure at the point when the compressor went unstable was nearly identical to point 1. Therefore, the predicted rotordynamic stability varied only slightly between the two con-

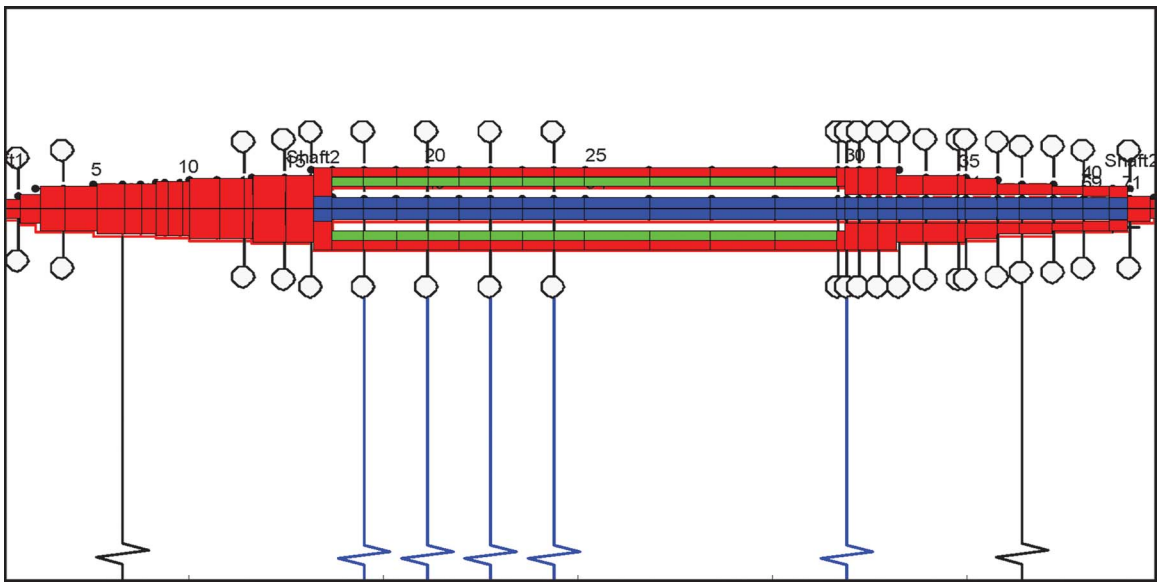

Fig. 3 Rotor beam model

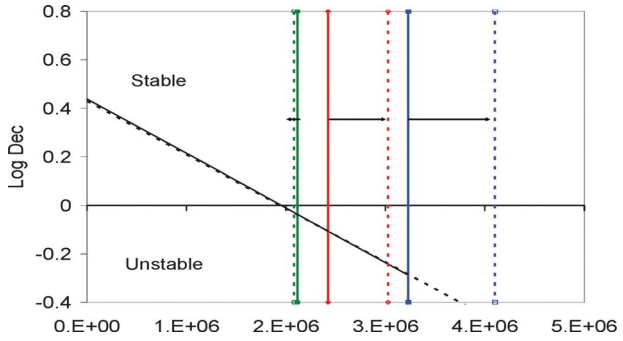

Fig. 4 Aerocross-coupling sensitivity of compressor rotor

ditions. For each case, the aerodynamic cross-coupling varied from 0 to about $4.0\times10^{+6}$, as shown in Fig. 4, to define the slope of the stability curve. The point where the lines intercept the vertical axis represents the system stability without the effects of aerodynamic cross-coupling ($K_{xy}=0$). The point where the sloped lines cross the horizontal axis is the stability threshold (log dec =0.0), beyond which the machine is predicted to be unstable. These two lines, identified as "Instability Pt. 1" and "Instability Pt. 2," demonstrate the sensitivity of the rotordynamic stability to midspan cross-coupling. Also, superimposed on this plot are the various predicted values of aerocross-coupling (vertical lines) using both of the Wachel variations discussed above, as well as the calculated SwRI–CFD results.

As shown in Fig. 4, both of the stability curves (instability points 1 and 2) cross the horizontal axis at about $2.0\times10^{+6}$ N/m aerocross-coupling. This identifies the amount of aerocross-coupling required from the impellers to reach an unstable condition. All other stabilizing and destabilizing parameters are included in this system characterization (i.e., impeller eye seals, balance piston seal, bearing coefficients, etc.). The API–Wachel method for calculating aerocross-coupling falls far to the right of the stability thresholds (points 1 and 2), indicating this method is overly conservative for this application. The SwRI–Wachel method falls even further to the right with an increased split between predictions for both instability points. On the other hand, the SwRI–CFD results show improved agreement in overall magnitude by closely matching the zero-crossing for both instability points. It is important to note that the SwRI–CFD results include only the cross-coupled stiffness (K_{xy}) from the analysis for a direct comparison to the other empirical methods. If the CFD predicted damping terms are included, the resulting aerocross-coupling will be decreased, possibly to a point below the stability threshold (i.e., instability not predicted). A more conservative approach is to leave out the damping term from the aerocross-coupling and use only the stiffness term for the design. This approach results in less computation time since only the eccentric, nonwhirling case needs to be modeled.

Also shown in Fig. 4, the experimental threshold shifts to the left slightly from point 1 to point 2 (increase in speed). The only calculation method to demonstrate the same trend is from CFD. In addition, this SwRI–CFD predicted shift is similar to experiment in magnitude, demonstrating that the fluid dynamic physics are being captured.

8 Additional Parametric Study Results

In an effort to better understand the application of this new formula, the authors continued their work by studying the effect of scale factor and impeller flow coefficient on the resulting cross-coupled coefficient (C_{mr}) [13]. The scale factor effect was studied by scaling an existing CFD impeller model to three times the original scale. The results demonstrated area scaling of the tangential forces, but the cross-coupled stiffness increased linearly with scale factor. As a result, the normalized coefficient for this single impeller remained unchanged. Table 3 provides a summary of the scale factor study results.

Table 3 Effect of scale factor [13]

	Original impeller	3X scaled impeller
F_t (N)	154	1390
ε (mm)	0.254	0.762
K_{xy} (kN/m)	608	1824
C_{mr}	7.1	7.1

It is also important to recognize that impellers can vary significantly in flow coefficient. The authors performed a CFD study to evaluate the influence of the flow coefficient on the resulting normalized coefficient. Flow coefficient is defined in Eq. (5) as

$$\phi = \frac{700.3Q}{ND^3} \tag{5}$$

where Q is the actual inlet flow (cfm), N is the speed (rpm), and D is the impeller diameter (in.).

The results presented so far have all been from a medium flow impeller, having a flow coefficient of 0.04. Figure 5 shows a generic example of impellers with different flow coefficients.

To cover this full range of likely impeller flow coefficients, the authors modeled two additional cases: one low flow coefficient impeller ($\varphi=0.02$) and one high flow coefficient impeller ($\varphi=0.15$). The low flow wheel was typical of multistage gas reinjection compressors and by design also included swirl brakes at the impeller eye seal location. The high flow wheel was more typical of LNG service. For both cases, CFD models were generated and solved at the design flow condition ($Q/Q_{\text{design}}=1.0$). Additionally, both models were run with swirl brakes (per design) and without swirl brakes. As a check on the overall results, impeller stage performance was compared with either the manufacturer's predictions or actual performance test results and was within 6% of the expected values. The dimensionless cross-coupled stiffness coefficient (C_{mr}) for the three impeller designs studied to date is summarized in Table 4. Note that the C_{mr} does not include the cross-coupling from the labyrinth seals, since the labyrinth seal remains concentric in the CFD model. The detailed geometry of the impellers was found to have an influence on the resulting cross-coupled stiffness for a given set of operating conditions. The effect of swirl brakes was more pronounced for short

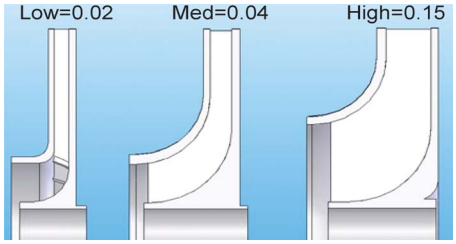

Fig. 5 Varying impeller flow coefficient example

Table 4 Summary of impeller cross-coupled coefficient results [13]

	φ	C_{mr} without swirl brake	C_{mr} with swirl brake	shroud clearance ratio
Low flow	0.02	4.08	1.24	0.027
Medium flow	0.04	7.30	N/A	0.027
High flow	0.15	4.44	4.04	0.019

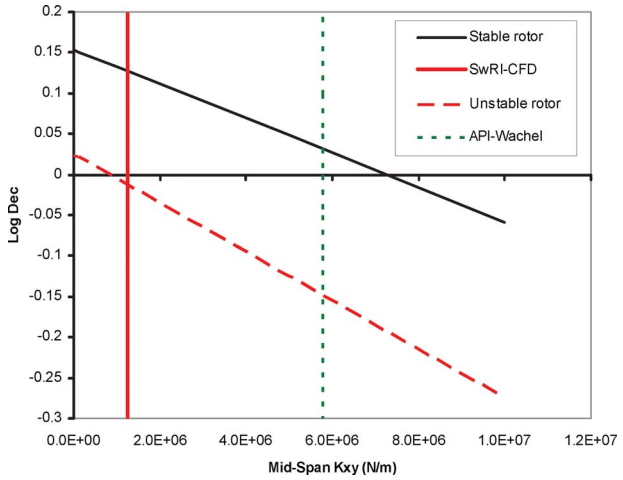

Fig. 6 Case study 1 stability plot

axial length stages like the low flow impeller, while minimal effect was observed for the high flow stage. The high swirl ratios presented in Table 2 helps to explain the larger C_{mr} value for the medium flow impeller. The swirl brakes are beneficial to not only reduce the cross-coupling from the impeller eye labyrinth seals but also reduce the cross-coupling from the impeller shroud force. This phenomenon can be explained by the reduction in swirl in the region adjacent to the labyrinth seal, which is also where the majority of the shroud passage cross-coupling is generated for lower flow coefficient impellers.

Table 4 also shows the ratio between the shroud passage and radial clearance normalized by the impeller radius at the tip. Since the low and medium flow impellers have an identical clearance ratio, clearance alone cannot explain the difference in C_{mr} between these two designs. The case for the medium flow with swirl brake was not computed.

9 New Case Studies

In an effort to further expand the database of impellers evaluated with this new method, the authors have accumulated the following case studies. In each of these, every effort has been made to apply what has been learned in a way that can be directly compared with the current state-of-the-art. Although CFD modeling of each case is not possible, this new method continues to demonstrate a more reliable attachment to the physics involved in generating the cross-coupled stiffness along the impeller shroud length. Proprietary restrictions prevent the authors from providing more geometric and operating condition data for these case studies.

9.1 Case Study 1: Back-To-Back Compressor. In this case study, a six stage back-to-back compressor is found to exhibit marginally stable behavior during full-load testing. The test results reveal greater than 10 μm of subsynchronous vibration. This is enough to be a concern, but certainly not enough to be considered a fully developed instability. The rotor is subsequently modified to increase the shaft stiffness, and the full-load testing is repeated. The repeat testing does not exhibit the subsynchronous vibration, demonstrating a successful attempt to eliminate the marginal instability.

Figure 6 is a plot of the rotor-bearing system logarithmic decrement versus the magnitude of impeller excitation (cross-coupled stiffness). The lower curve (starting at log dec <0.05) shows that the system crosses into the unstable region at very low excitation values. This curve represents the original rotor design. The upper curve (starting at log dec ≈ 0.15) demonstrates less sensitivity to impeller excitation, crossing into the unstable region at $7.0 \times 10^{+6}$ N/m. This curve represents the modified rotor with increased shaft stiffness.

The vertical lines in Fig. 6 represent predicted impeller excitation values based on two different methods. The right vertical line ($\approx 5.8 \times 10^6$ N/m) is from the current API–Wachel formulation and detailed calculations are provided in Table 5. The left vertical line ($\approx 1.3 \times 10^6$ N/m) is a result of the current SwRI–CFD model, with detailed calculations provided in Table 6. Although CFD analysis was not performed for this particular impeller design, the C_{mr} coefficient was given a value of 4.4. Included in Table 6 is the value of the flow coefficient for each wheel, and it is clear from these numbers that these are fairly high flow impellers. Based on the results of the impeller sensitivity study, it is reasonable to use the C_{mr} number associated with high flow wheels.

Note that by using the current API–Wachel standard for impeller excitation, the log dec of the original rotor is shown to be significantly below the stability threshold with a log dec of about -0.15. The modified rotor is shown to be marginally stable with log dec <0.05. However, with the SwRI–CFD impeller excitation model, the original rotor is shown to be only marginally unstable (log dec >-0.05), and the modified rotor is shown to be clearly stable with a predicted log dec >0.10.

Log dec predictions in the 0.05 range are certainly suspected given the potential uncertainty in these analyses. However, it is generally accepted that predictions above the 0.10 range are considered more reliable. Therefore, it is reasonable to conclude the following:

- Using the API–Wachel method, the original rotor is predicted to be clearly unstable, while the modified rotor is predicted to be marginally stable, at best.
- Using the SwRI–CFD method, the original rotor is predicted to be marginally stable, while the modified rotor is predicted to be stable, with log dec >0.10.

Table 5 API–Wachel calculation results

	API–Wachel					
	Stage 1	Stage 2	Stage 3	Stage 4	Stage 5	Stage 6
C	9.55	9.55	9.55	9.55	9.55	9.55
Power (W)	$5.43 \times 10^{+6}$	$5.64 \times 10^{+6}$	$5.61 \times 10^{+6}$	$4.24 \times 10^{+6}$	$4.31 \times 10^{+6}$	$4.18 \times 10^{+6}$
B_c	3.00	3.00	3.00	3.00	3.00	3.00
D (mm)	1010	1010	1000	880	880	880
B_3 (mm)	58	54	49.5	46.5	43	39.3
ρ_d (kg/m^3)	21.78	25.45	29.63	37.24	42.22	47.42
ρ_s (kg/m^3)	19.15	22.30	26.12	33.46	38.02	43.08
K_{xy} stage (N/m)	$8.39 \times 10^{+5}$	$9.39 \times 10^{+5}$	$1.02 \times 10^{+6}$	$9.18 \times 10^{+5}$	$1.01 \times 10^{+6}$	$1.06 \times 10^{+6}$
K_{xy} TOT (N/m)			$5.78 \times 10^{+6}$			

Table 6 SwRI–CFD calculation results

	SwRI–CFD					
	Stage 1	Stage 2	Stage 3	Stage 4	Stage 5	Stage 6
C_{mr}	4.4	4.4	4.4	4.4	4.4	4.4
ρ_d (kg/m^3)	21.78	25.45	29.63	37.24	42.22	47.42
U (m/s)	190.44	190.44	188.56	165.93	165.93	165.93
D (m)	1.01	1.01	1	0.88	0.88	0.88
L_{shr} (m)	0.1457	0.1452	0.1405	0.129	0.1271	0.1197
Phi	0.092	0.080	0.071	0.084	0.075	0.067
K_{xy} stage (N/m)	$4.85\times10^{+5}$	$5.90\times10^{+5}$	$6.63\times10^{+5}$	$5.52\times10^{+5}$	$6.23\times10^{+5}$	$6.01\times10^{+5}$
Modal weight	0.523	0.616	0.656	0.648	0.597	0.509
K_{xy} stage weighted (N/m)	$1.33\times10^{+5}$	$2.24\times10^{+5}$	$2.86\times10^{+5}$	$2.32\times10^{+5}$	$2.22\times10^{+5}$	$1.56\times10^{+5}$
K_{xy} TOT (N/m)			$1.25\times10^{+6}$			

It is also important to understand the sensitivity of the SwRI–CFD method to the "correct" value of C_{mr}. In this case, the value of 4.4 was used due to the high flow coefficient design of the impellers. The range of C_{mr} values currently in the public domain is 4.0–7.3 [13]. If this particular case is evaluated at both of these extremes, the resulting net impeller excitation is calculated to be $1.14\times10^{+6}$ N/m and $2.08\times10^{+6}$ N/m for the minimum and maximum values, respectively. Referring to Fig. 6, it is clear that the overall conclusions on rotor system stability are not altered by this full range of values.

Clearly, in this case, the current method leads to conclusions that more accurately represent the actual experience with the original and modified rotor designs. This is an encouraging result, suggesting that this new approach can allow the compressor design community to improve rotordynamic stability predictions as the database of C_{mr} values matures.

9.2 Case Study 2: Straight-Through Compressor. The second case study investigates a low pressure (LP), eight-stage straight-through compressor used for offshore gas re-injection. The compressor contains all labyrinth seals through the machine with a swirl brake on the balance piston seal. The low flow CFD case shown above comes from its sister high pressure compressor, which operates in series. While the compressor has a discharge pressure of only 74 bar, the rotor is relatively flexible given the eight stages. The cross-coupling is computed with three methods as before. The stability is studied both with and without swirl brakes on half of the impeller eye seals. As previously shown, swirl brakes benefit stability by not only reducing the swirl entering into the impeller seal, but also by reducing the impeller cross-coupling. Figure 7 shows the resulting stability plot for both swirl brake and no swirl brake cases. Notice that the SwRI–CFD cross-coupling decreases with the addition of the swirl brakes, while the API–Wachel value makes no distinction between the two. The predicted log dec is similar using both the SwRI–CFD and the API–Wachel values with no swirl brakes. However, with swirl brakes, SwRI–CFD predicts log dec=0.25 while the API–Wachel level of cross-coupling predicts 0.18. Both satisfy the API 617 [5] stability requirement of 0.1 for this case. This compressor currently is awaiting field commissioning.

10 Conclusions

This study works to develop an improved methodology to predict the cross-coupled stiffness of centrifugal impellers for a variety of geometry and operating conditions. The analytical method developed in this study utilizes CFD to predict the rotordynamic forces using a variety of impeller geometry and operating conditions. This work led to the development of a new analytical formula that appears to better capture the true physics of the problem compared with methods currently used. An unstable compressor case study is used to validate the method and demonstrates that both the impeller shroud and eye seal coefficients are needed to explain the instability. Both case studies presented clearly show that labyrinth seal forces alone cannot explain the unstable behavior observed experimentally. Therefore, the authors advocate that an impeller shroud model in addition to modeling the labyrinth seals should be employed when performing a level 2 API 617 [5] analysis.

The results show a dependency of the nondimensional impeller cross-coupling coefficient (C_{mr}) on impeller flow coefficient, as well as the presence of swirl brakes. The normalizing equation presented by Moore et al. [12] provides reasonable results when used to scale CFD results within a family of impellers. However, some differences exist even when the same impeller is used for different gases. This demonstrates that there may be additional factors that affect the cross-coupling such as the swirl distribution along the impeller shroud passage and shroud clearance. Clearly, only CFD is capable of capturing these subtle effects. The dimensionless coefficients presented here may be used as an improved approximation for the cross-coupled stiffness for different classes of impeller over the Wachel based formulas. However, for best accuracy, the authors advocate performing a CFD analysis on at least one stage from each impeller family using the field gas conditions.

Acknowledgment

The team would like to thank Southwest Research Institute for providing the funding, software, and computing platform required for this research.

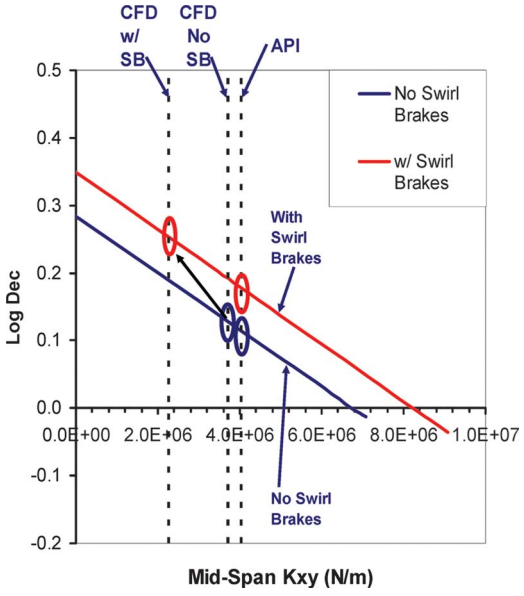

Fig. 7 Case study 2 stability plot

Nomenclature

B_c = API–Wachel centrifugal compressor coefficient
B_3 = diffuser passage width (in.) (m)
C = API–Wachel coefficient
C_{mr} = impeller cross-coupling coefficient
D = impeller diameter (in.) (m)
Hp = stage power (hp) (kW)
k_{xy} = cross-coupled stiffness of each impeller (lbf/in.) (N/m)
K_{xy} = modal sum of cross-coupled stiffness (lbf/in.) (N/m)
L_{shr} = axial length of shroud from impeller eye seal to impeller tip (in.) (m)
MW = gas molecular weight
N = rotor speed (rpm)
Q/Q_{design} = flow relative to design (best efficiency point) flow
U = impeller tip speed (ft/s) (m/s)
WFR = whirling frequency ratio, Ω/ω
WFR_s = whirling frequency ratio at instability
η = impeller modal amplitude for the first mode of vibration (peak amplitude normalized to one)
ρ_d = stage discharge density (lbm/ft^3) (kg/m^3)
ρ_s = stage suction density (lbm/ft^3) (kg/m^3)
ω = impeller rotational speed (rad/s)
Ω = impeller precession frequency (rad/s)

References

[1] Memmott, E. A., 2000, "Empirical Estimation of a Load Related Cross-Coupled Stiffness and the Lateral Stability of Centrifugal Compressors," CMVA, *Proceedings of the 18th Machinery Dynamics Seminar*, Halifax, Canada, pp. 9–20.
[2] Moore, J. J., and Palazzolo, A. B., 2001, "Rotordynamic Force Prediction of Centrifugal Impeller Shroud Passages Using Computational Fluid Dynamic Techniques With Combined Primary/Secondary Flow Model," ASME J. Eng. Gas Turbines Power, **123**, pp. 910–918.
[3] Moore, J. J., and Palazzolo, A. B., 1999, "CFD Comparison to 3D Laser Anemometer and Rotordynamic Force Measurements for Grooved Liquid Annular Seals," ASME J. Tribol., **121**(2), pp. 306–314.
[4] Wachel, J. C., and von Nimitz, W. W., 1980, "Assuring the Reliability of Offshore Gas Compression Systems," European Offshore Petroleum Conference and Exhibition, London, England.
[5] API 617, 2002, *Axial and Centrifugal Compressors and Expander-Compressors for Petroleum, Chemical and Gas Industry Services*, 7th ed., American Petroleum Institute, Washington, DC.
[6] Baun, D. O., 2000, "Measurement and Prediction of Impeller Forces in a Single Volute Pump," Ph.D. thesis, University of Virginia, Charlottesville, VA.
[7] Childs, D., 1989, "Fluid-Structure Interaction Forces at Pump Impeller-Shroud Surfaces for Rotordynamic Calculations," ASME J. Turbomach., **111**, pp. 216–223.
[8] Gupta, M., and Childs, D., 2007, "New Steps to Improve Rotordynamic Stability Predictions of Centrifugal Compressors," ASME Paper No. GT2007-27501.
[9] Fulton, J., 2003, "Rotor Stability Criteria for Multi-Stage Centrifugal Compressors," *Proceedings of the ASME International Design Engineering Technical Conference*, Chicago, IL, 5B, pp. 1327–1336.
[10] Gupta, M. K., Soulas, T. A., and Childs, D. W., 2008, "New Steps to Improve Rotordynamic Stability Predictions of Centrifugal Compressors," ASME J. Eng. Gas Turbines Power, **130**(2), p. 022505.
[11] Moore, J. J., 2003, "Three-Dimensional CFD Rotordynamic Analysis of Gas Labyrinth Seals," ASME J. Vibr. Acoust., **125**, pp. 427–433.
[12] Moore, J. J., Ransom, D. L., and Viana, F., 2007, "Rotordynamic Force Prediction of Centrifugal Compressor Impellers Using Computational Fluid Dynamics," ASME Paper No. GT2007-28181.
[13] Moore, J. J., and Ransom, D. L., 2008, "Refinement of Physics Based Approach Used in the Prediction of Impeller Rotordynamic Forces for Centrifugal Compressors," ASME Paper No. GT2008-51484.
[14] Moore, J. J., 1999, "Rotordynamic Force Prediction of Whirling Centrifugal Impeller Shroud Passages Using a Combined Primary/Secondary Passage Model," Ph.D. thesis, Department of Mechanical Engineering, Texas A&M University, College Station, TX.
[15] 2006, ANSYS CFX-5 User's Manual, ANSYS, Inc., Canonsburg, PA.
[16] 2006, XLTRC^2 User's Manual, Texas A&M University, College Station, TX.